West Virginia University
High Altitude Cosmic Radiation (HACR) Detector
Payload Summary and Flight Science Report

Department of Mechanical and Aerospace Engineering
West Virginia University, Morgantown, WV 26506/6106

12/20/2007

Submitted by: WVU Team HACR

Student Members:
John H. Brewer, III
Nicholas J. Hansford
Jeremy C. Hill

Faculty Members:
Dr. G. Michael Palmer
Dr. John M. Kuhlman

Abstract

A package to measure the cosmic ray intensity using two plastic scintillation detectors coupled to photomultiplier tubes positioned along the gravity gradient was designed, built, tested, and flown on the High Altitude Student Payload (HASP) platform on September 2, 2007 from the Columbia Balloon Flight Facility Fort Sumner, NM facility. The data for this flight was analyzed and a simple model was developed and used to fit the data.

Measurements of the relative cosmic ray intensity along the gravity gradient and isotropic intensity were observed as the HASP platform moved from ground level to a nominal float altitude of 120,000 ft. The intensity of the cosmic rays was observed to vary from ground to 120,000 ft as other investigators have reported. A maximum in intensity (counts per second) occurred at an altitude of 55,000 ft or at about 110 g/cm^2. The shape of the observed coincidence curve was in good agreement with previous investigations. A complete set of data for the HASP entire duration of the flight was not obtained due to electronic problems.

Table of Contents

Page #

Table of Figures

Table of Tables

Table of Equations

Introduction

Cosmic radiation was first detected in 1912 by Victor Hess during a balloon flight at 16,000 feet (1). Since that time, cosmic radiation has been studied by many, using various types of detectors for various lengths of time. This type of radiation was thoroughly studied during the early stages of the US Space Program to determine the risk to spacewalking astronauts. Recently, however, it has been suggested by several in the aviation and medical communities that the affects of cosmic radiation are broader than one would expect. The primary concern in these communities is for people that spend a large amount of time flying at commercial flight altitudes, such as aircraft crews. In response to the increased risk from cosmic radiation, the US Federal Aviation Administration (2), the World Health Organization (3), and the European Union (4) have made recommendations regarding exposure levels for pregnant aircrew. A secondary concern by those in the aviation community is the probability of a Single Event Upset (SEU) causing a major system failure in an aircraft avionics (5).

This study was conducted in an attempt to experimentally confirm the Pfotzer curve (cosmic ray intensity vs. altitude or atmospheric density). This was done by measuring the intensity of cosmic rays along the gravity gradient and in spherical geometry in the upper atmosphere. It was also hoped that there would be a measurable change in cosmic radiation with the change in solar radiation; however, this was not accomplished due to electronic problems.

Theory

Basic Model

The origin of cosmic rays is somewhat unknown, but is believed to be the result of galactic supernovae. As cosmic rays enter the Earth's atmosphere, they interact with air molecules producing particle cascades, known as cosmic ray showers. Figure 1 shows the production of a shower by a single ray. As these showers progress through the atmosphere, the energy of the ray is transferred to the various subatomic particles and electromagnetic rays that are produced in each interaction or lost to thermal energy.

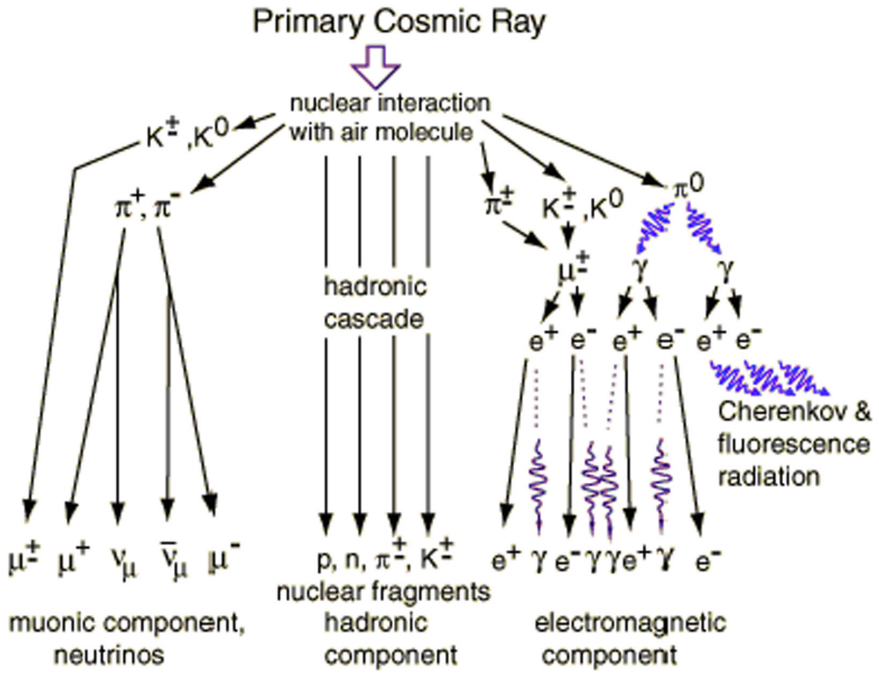

Figure 1: Cosmic Ray Shower Model (6)

WVU Model[1]

As the cosmic rays enter the earth's atmosphere they interact with air in a number of ways. If the atmosphere were of constant density the change of comic rays flux,Φ, measured in number/sec/area per unit of distance would be given by:

$$d\Phi / dh = -\mu\Phi ,$$

Equation 1: Change of Cosmic Ray Flux for Constant Density

where h is the measure of vertical distance and μ is a constant expressing the probability that a cosmic ray will interact with an atmospheric element such as to remove it from the flux. When this is integrated over h the flux as a function of distance becomes:

$$\Phi(h) = \Phi_o \exp(-\mu h),$$

Equation 2: Integrated Cosmic Ray Flux

where Φ_o is the initial flux at h = 0 and Φ(h) is the flux at some distance greater than zero.

In the case of the Earth's atmosphere the density varies as a function of altitude, which requires a second part be added to the above function for Φ(h). If μ is no longer considered constant but is replaced by:

$$\mu(h) = \mu_0 + \mu_0\rho(h)/\rho_o ,$$

Equation 3: Non-constant Atmospheric density

where μ_o and ρ_o are the value of μ and ρ at some arbitrary altitude.

[1] Developed by Dr. G. Michael Palmer, Emeritus Professor of Mechanical and Aerospace Engineering at West Virginia University.

Then the change in flux with altitude will be expressed by:

$$d\Phi/dh = - \mu(h)\Phi,$$

Equation 4: Change in Cosmic Ray Flux for Variable Density

Integrating this gives the result:

$$\Phi(h) = \Phi_0 \exp[-\mu_0(h - h_{\max})]\exp\left[-\mu_0/\rho_0 \int_{h\max}^{h} \rho(h)dh\right]$$

Equation 5: Integrated Cosmic Ray Flux for Variable Density

Here h_{max} is a very high altitude, here taken as 125,000ft and $\rho(h)$ is air density as a function of altitude. Letting $k_1 = \mu_o$, $k_2 = \mu_o/\rho_o$, and $\Phi_{max} = \Phi_o$ and noting that interaction events are the product of $\Phi_{max}\,\rho(h)$ one obtains:

$$counts = \Phi_{\max} * \rho(h) * \exp(-k_1 * (h_{\max} - h)) * \exp(-k_2 * \int_{h\max}^{h} \rho(h)dh)$$

Equation 6: Count Rate Model

Using the present coincidence data the optimal values of k_1, k_2, and Φ_{max} were found to be:

$k_1 = 2.6\text{x}10^{-5}$ ft $^{-1}$

$k_2 = 8.5\text{x}10^{-2}$ ft ^{2} slug $^{-1}$

$\Phi_{max} = 8.5\text{x}10^6$ events

These values were obtained by doing a numerical integration over $\rho(h)$ dh to find the count at any given altitude and a numerical least-squares fit to the data. These are the data that is plotted in Figures 10 and 11. The data for atmospheric density were calculated by conversion of the fitted data to cgs units.

Apparatus

Detector

The detector used in this experiment was a plastic scintillation detector produced by Saint-Gobain Crystals of Newbury, Ohio. This type of detector was chosen because of its lightweight and reliability. The scintillation material selected for the detector was the BC-408 plastic scintillator. Ideally, this detector would have used Sodium Iodide (NaI (TI)) crystals because of their high output, rapid response rate, and sensitivity over a broad range of energies. However, Sodium Iodide was rejected due to its high density and the one-kilogram total weight limit on our payload. The BC-408 plastic scintillator was selected primarily for its low density and faster response rate than the Sodium Iodide. The BC-408, however, has a smaller spectrum of energy sensitivity and is a less efficient scintillator, averaging only about 25% of the light output of NaI (TI).

The detectors were configured as shown in figure 2, with the scintillator paddles mounted to photomultiplier tubes (PMT). These tubes were manufactured by Hamamatsu Photonics and were model number R1924A. This tube model was selected because its maximum cathode sensitivity occurred near the 425nm maximum emission wavelength of the BC-408 scintillator. These tubes were rated to withstand the thermal and shock loading that was anticipated to be present during different phases of the balloon flight.

The tubes were optically and physically mounted to the center of the scintillator paddles and in opposite directions so as to meet the payload maximum height requirements set forth by the overseeing balloon flight organization at Louisiana State University. This configuration also allowed for the construction of an inner foam payload container to secure the tubes and paddles such that they would not be at risk of damage in the event of a hard landing or impact during flight. Figure 3 shows one of the two light tight detector assemblies. It was essential that no light be allowed to enter the detector because this light would have been significantly more powerful than the light emitted by the BC-408 plastic and thus would have blinded the detector.

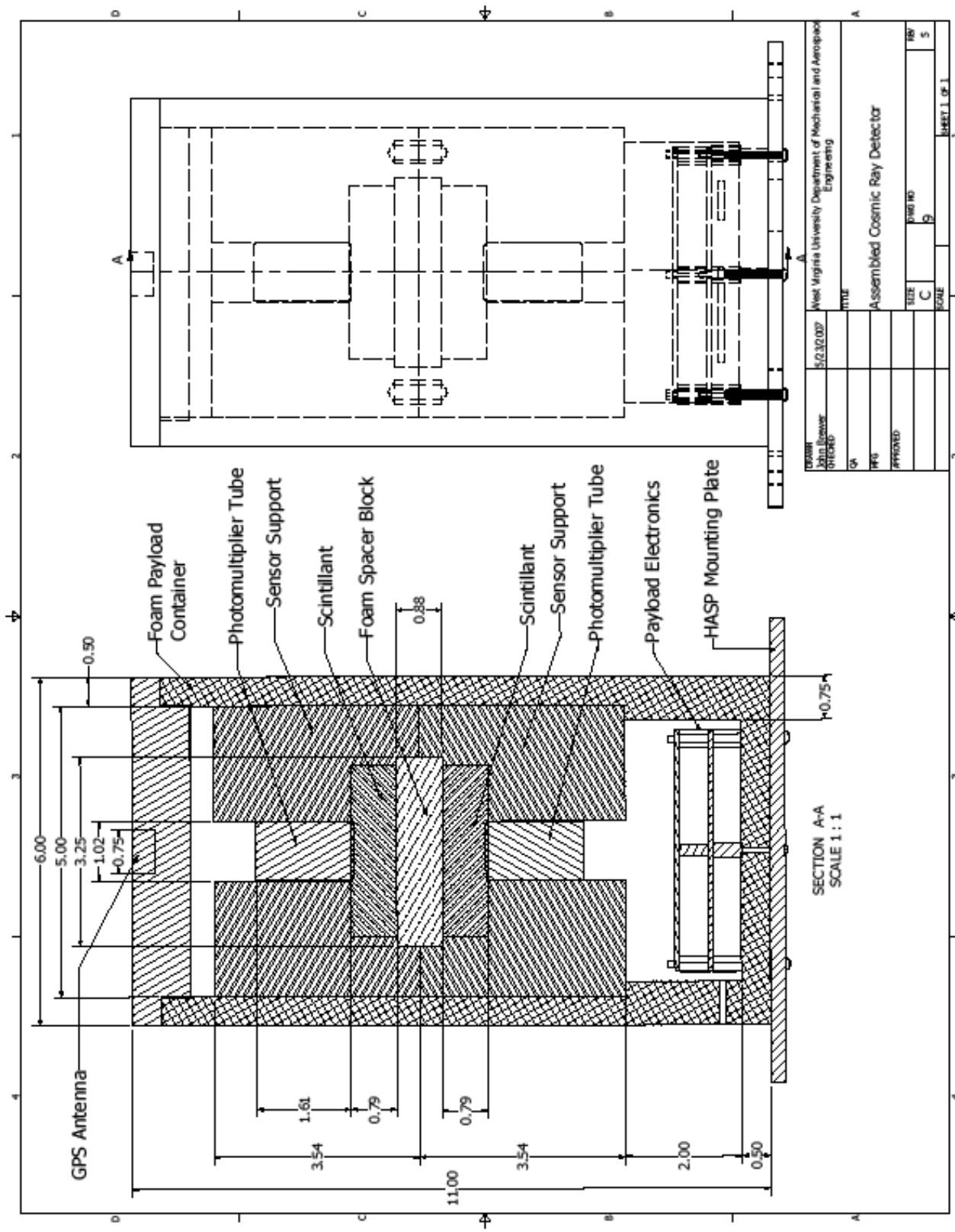

Figure 2: WVU HASP Payload Diagram

Figure 3: Single Light Tight Detector Assembly

System Electronics

Power System

Figure 4 is a diagram of the internal power supply circuit used by the payload. Power was supplied from the HASP platform through an EDAC-516 connection. The HASP platform supplied the small payload packages with a nominal 28 Volts (24 to 32V) and up to 500 mA, or about 14 Watts. This voltage was too high for linear regulators to the lower voltages.

12 Volt Supply

The 28 Volt was first converted to 12 Volts using a high efficiency DC-DC converter (PWR1 in Figure 4). This converter could supply 12 Volts up to 1000 mA (about 12 Watts) with an efficiency of 85%. This voltage is monitored on analog channel 1 of the CPU on 0 to 4.096 Volts scaled to one-fourth the voltage by voltage divider R8, R7.

+5 Volt Supply

The CPU and other sections of the instrumentation required regulated 5.0 Volts. The most convenient way to get this voltage was from the 12 Volt supply via a linear regulator (VR1 in Figure 4). Since the 5 Volt power requirements would be only a few 10's of mA the use of a DC-to-DC converter was rejected because of added weight and cost. This voltage is monitored on analog channel 0 of the CPU on 0 to 4.096 Volts scaled to one half the voltage by voltage divider R4, R5

-5 Volt Supply

The voltage comparators in the PMT circuits need a bipolar supply voltage. To get a negative 5 Volts a charge pump voltage doubler (LT1026 5 to –10 Volt) was used. This voltage was then stabilizer (regulated) to –5Volts with VR3 (Figure 4). The +5V and the –5V supplies then provided the required bipolar voltages.

3.3 Volt Supply

The data storage card and the GPS receiver required 3.3 Volts. This was obtained from the 5 Volt supply using a linear regulator (VR2 in Figure 4). This voltage is monitored on analog channel 1 of the CPU on 0 to 4.096 Volts scale.

1250 Volt Supply

The photomultiplier tubes require a very stable positive voltage in the range of 500 to 1500 Volts at very low current (few hundred nA). A DC to DC converter in the 0 to 1500V range designed for PMT use was used for this power supply. A 10 kΩ adjustable resistor (R2 in Figure 4) allowed the voltage to be set to the desired value.

4.096 Volt Reference Supply

The 10- bit analog to digital (ADC), which is part of the CPU, requires a reference voltage. The WVU HASP board uses an Analog Devices REF198 (U2 in Figure 4) to provide 4.096 Volts to the reference input. This IC provides a highly accurate and stable reference voltage.

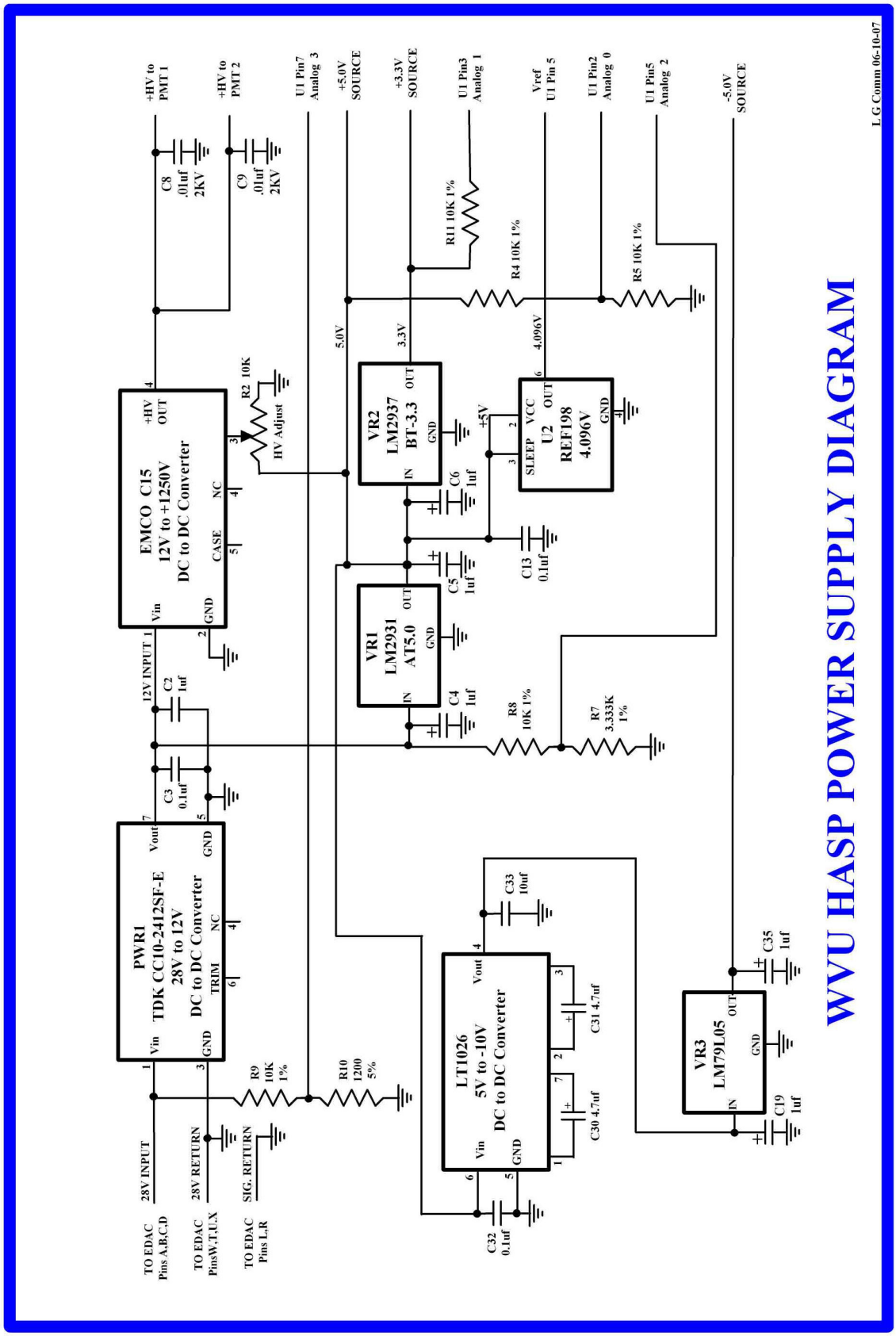

Figure 4: WVU HASP Power Supply Diagram

Central Processing Unit

A Microchip PIC18F2525-I/P microprocessor was used to acquire data, store data, and communicate with the HASP platform. Four data streams (pulse data) from the PMTs were connected to 4 inputs of the CPU. The remaining channels were used to read voltage, temperature, GPS data, and communicate with the HASP platform. Table 1 shows the list of data channels and their use.

Table 1: CPU Data Streams

RA0	5 Volt supply
RA1	3.3 Volt supply
RA2	12 Volt supply
RA3	4.096 Voltage Reference
RA4	External Package LED
RA5	28 Volt supply
RB0	Channel A AND Channel B data
RB1	Channel B PMT data
RB2	Channel A PMT data
RB3	GPS Data In
RB4	GPS Data Out
RB5	Channel A AND Channel B delayed data

Temperature System

The temperature was measured two places within the HASP package. One sensor was located adjacent to the 1500 Volt PMT power supply and called the 'Board Temperature' and the second sensor was located at the top of the detector package and inside the outer insulating cover and referred to as the 'Box Temperature'. Data from these sensors was recorded at the end of each 10-second count period and stored as part of the data record on the Data Flash card.

The temperatures were measured with LM34 solid-state temperature sensors. These sensors have an analog output of 10mV/°F with bipolar output. The analog signals from these sensors were connected to two 13-bit differential input two-channel ADC (Microchip MCP3302) with a range of –2.048 to +2.048 Volts providing about –200 to +200 °F range.

GPS System

A Trimble Lassen SQ 8-channel GPS receiver and unpackaged patch antenna were located within the top cover of the HASP package and connected to the main board via a cable with power (3.3V), Ground, Serial Transmit data, and Serial Receive data. The two data lines from the GPS were connected to CPU ports RB3 and RB4 through two buffers (U7C andU7D). The buffers provide level conversion 3.3V to 5V logic. Data in the form of the NEMA GGA GPS sentence are recorded at the end of the 10 second data period and written to the Data Flash card as a field of the period data record. The important data fields are position, time, altitude, and number of satellites seen.

A software serial port is implemented in the PIC18F4620 to support the GPS receiver at 4800 Baud. The GPS receiver sends a $GPGGA sentence every second to the CPU. This most recent data is parsed and checked for validity when data storage is requested.

Communications System

The CPU hardware serial port was used for the 1200 Baud communication with the HASP system during the flight. An ASCII data packet was transmitted to the HASP platform every 10 seconds using standard RS-232 levels. This interface could, but was not, used for receiving command data from the HASP system. Configuration data for the WVU HASP board was also communicated via this port. The board was placed in configuration mode using jumper JU2. A short on JU2 (jumper block on) indicated test or configuration mode and JU2 open indicates normal operation. The CPU had to be restarted to make mode changes. In configuration mode the interface runs at 19,200 baud.

During the HASP integration session an RS-232 level converter was added to conform to the levels required by the HASP system. The level converter translates 5V TTL levels provided by the board to the ±10V RS-232 levels. A photo of the added board is given in figure 5.

The transmitted data was formatted into 218 bytes in length and formatted as shown in Table 2. The data was structured in such a way as to prevent string splitting by the ground station as it parsed received packets into files during the flight. Onboard data was stored in binary format. Transmitted data was sent in ASCII format such that when viewed on the ground during the flight, proper payload function could be verified.

Table 2: WVU HASP Data Structure

Field	Data	Size (bytes)
1	Payload Identifier	30
2	Point Number	8
3	Channel A count	10
4	Channel B count	10
5	Channel A*B count	10
6	CPU Temperature (˚C)	8
7	Internal Payload Temperature (˚C)	8
8	ADC code 5V Buss	8
9	ADC code 3.3V Buss	8
10	ADC code 12V Buss	8
11	ADC code 28V Buss	8
12	GPS data	100
13	Carriage Return – Linefeed	2
	Total Size:	218

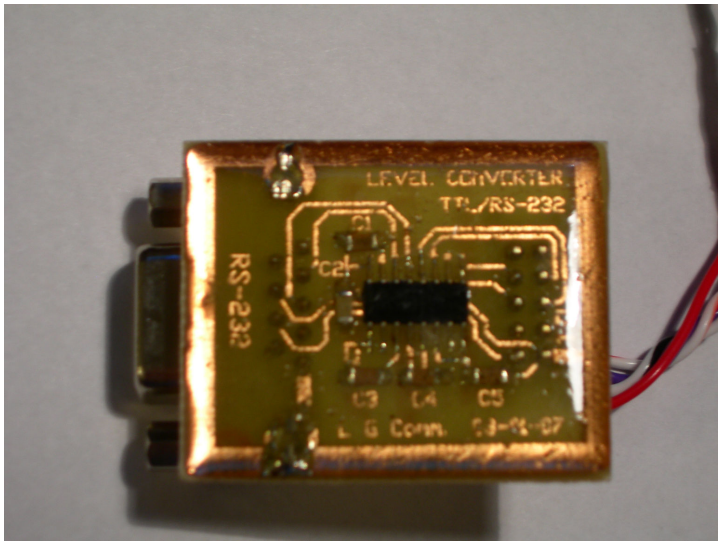

Figure 5: WVU HASP TTL to RS-232 Level Converter

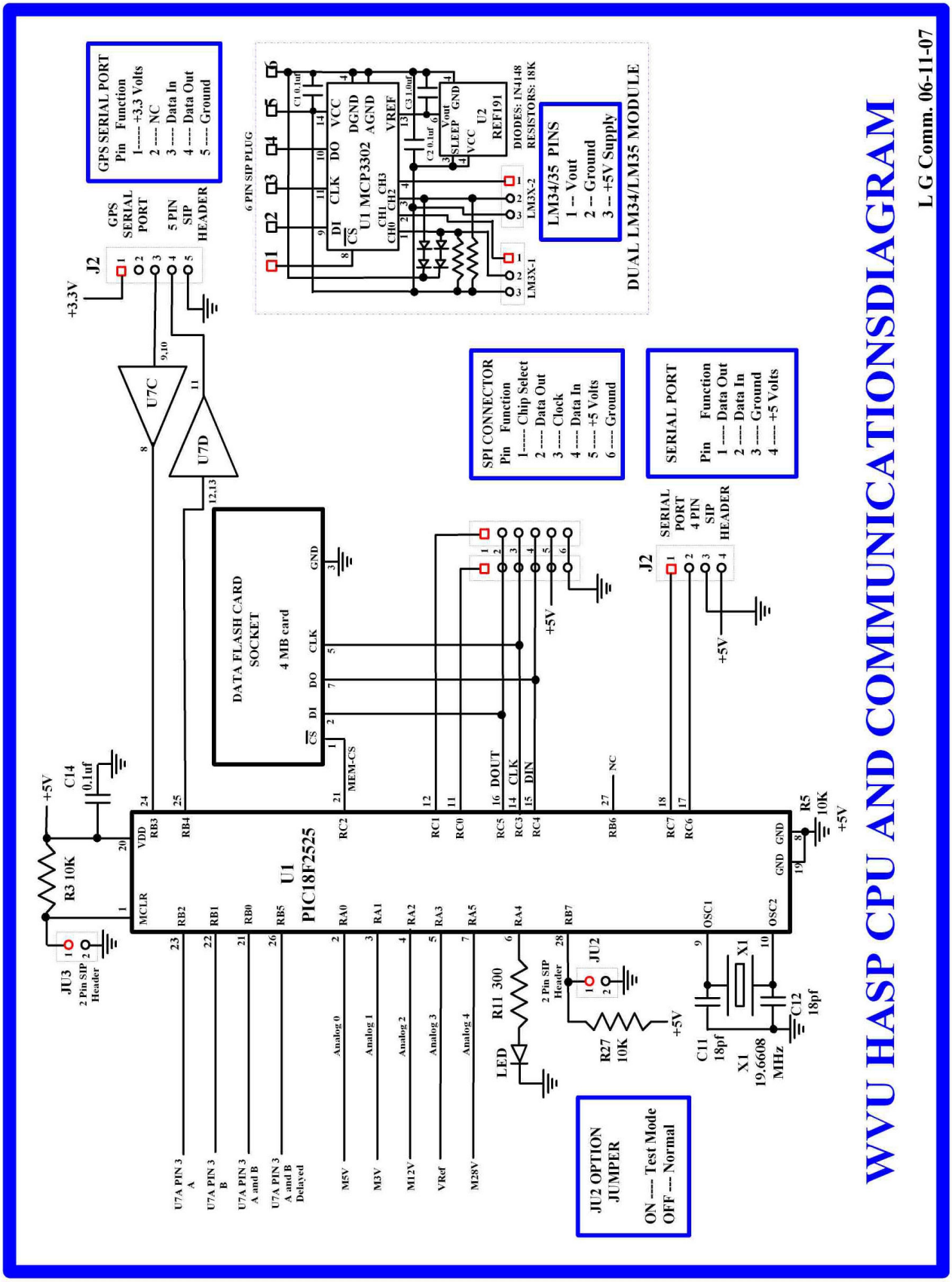

Figure 6: WVU HASP CPU, Communications and Temperature Circuit Diagrams

Photomultiplier Interface

Figure 7 shows the photomultiplier tube interface (coincidence) circuit. This circuit accepts input signal from the photomultiplier sockets and through a series of logical operations outputs whether the signals were coincident, single, or accidental. The output from each photomultiplier tube was first run into a 7ns comparator (AD8561) with a 10K level set resistor. The output from each comparator was then run into a single shot multivibrator of 750ns fixed length, which was set using a 10kΩ resistor and a 100 pF capacitor. This output signal was found to have some noise that was introduced by the comparators, and thus capacitors were added between the multi-vibrators and the comparators to filter this noise.

The output from the multi-vibrators was then run into the branching circuit where coincidence was determined. This circuit was branched into four separate channels. The channel A and B data are referred to as the 'singles' counts on the respective PMT input. The A AND B counts are the coincidence counts and the A AND Delayed B is referred to as the 'accidental' counts. These data were counted for and recorded every 10 seconds. This then allows the observation of the 10-second count rate and cumulative counts on each of the channels.

For A AND B data to be 'in coincidence', an event must be registered by each detector within 1.5μs of each other (2τ = 1500 ns). Such events are assumed to be due to the same cosmic ray event passing through both detectors, and therefore as having traveled along the gravity gradient. There is a possibility that two non-related events may be counted as coincident events if they arrive with in the 2τ-time window. Correction for these accidental events may be made by recording coincidence events artificially separated in time, or A AND Delayed B, where the Channel B has a large delay a with respect to τ . This data was recorded on the fourth data channel as accidental counts.

The accidental count rate should be related to the A and B count rates (singles) by the relationship:

$$N_{ACC} = 2\tau N_A N_B ,$$

Equation 7: Accidental Count Rate

where N_{Acc}, N_A, and N_B are accidental, channel A and channel B count rates respectively in units of counts per second and τ is in seconds. This relationship was confirmed for our instrument using Co^{60} and Na^{22}. Using in-flight data A and B rates of $\approx$140 counts/sec. and τ = 750ns = 7.5 x 10^{-7}sec the measured accidental rate should be about 0.03 counts per second or 0.3 counts in ten seconds. This is very close to what was observed.

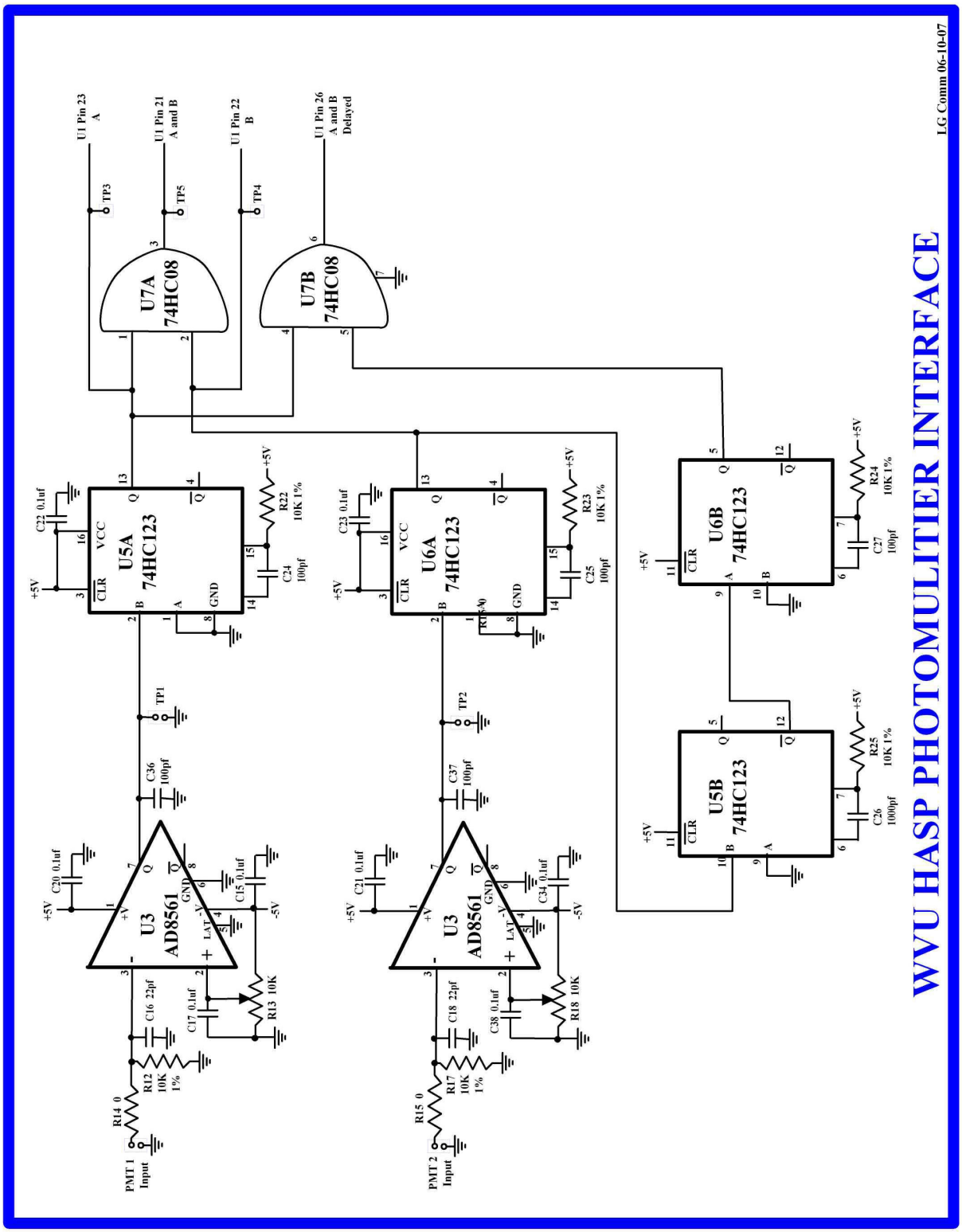

Figure 7: WVU HASP Photomultiplier Interface

Systems Bill of Materials

MAIN:

Item	Count	Label-Value	Pattern	Designation(s)
1	1	GND	SIP3	GND
2	1	TP1	SIP2	TP1
3	9	10K 1%	SM1206_b	R4,R5,R7,R12, R17,R22,R23,R24, R25
4	14	0.1uf	SM1206_b	C1,C3,C14,C15, C17,C20,C21,C22, C23,C28,C29,C32, C34,C38
5	1	TP6	SIP7	TP6
6	1	JU2	RAD0.1	JU2
7	1	Jumper	AXIAL0.3	J
8	1	JU1	RAD0.1	JU1
9	10	Jumper	SM1206_b	J,J,J,J,J, J,J,J,J,J
10	1	RED LED	RAD0.1	LED1
11	1	SPIB	SIP6	SPIB
12	1	SPIA	SIP6	SPIA
13	4	Jumper	RAD0.2	J,J,J,J
14	3	10K	SM1206_b	R3,R6,R27
15	1	1.0uf	SM1206_T	C10
16	1	0.1	SM1206_T	C13
17	3	10K 15T POT	VR4	R2,R13,R17
18	1	0.01uf/2KV	AXIAL0.4	C9
19	1	0.01uF/2KV	AXIAL0.4	C8
20	1	LM7805	TO-220	VR1
21	1	MEM CRD	ATMEL+DF_2	MC
22	1	COMM	SIP4	JCOM
23	1	19.6608MHz	XTAL1	X1
24	4	100pf 5%	SM1206_b	C24,C25,C27,C37
25	4	22pf 5%	SM1206_b	C11,C12,C16,C18
26	2	AD8561AN	DIP8	U3,U4
27	2	74HC123	DIP16	U5,U6
28	2	10uf	SM1206_b	C2,C33
29	1	100pf	SM1206_b	C36
30	2	4.7uf	SM1206_b	C30,C31
31	1	PMT1	SIP2	PMT1
32	1	PMT2	SIP2	PMT2
33	1	PIC18F2525	DIP28.3X1500	U1
34	1	1000pf 5%	SM1206_b	C26
35	1	LM2937ET-3.3	TO-220	VR2
36	6	1.0uf	SM1206_b	C4,C5,C6,C7, C19,C35
37	1	3.333K 1%	SM1206_b	R8
38	1	10K 1%	SM1206_T	R9
39	1	1200 5%	SM1206_T	R10
40	1	GPS	SIP5	JGPS
41	1	330	SM1206_b	R11
42	1	74HC08	DIP14	U7
43	1	JU3	RAD0.1	JU3
44	1	LM79L05	TO-92A	VR3

45	2	0 Ohm	SM1206_b	R14,R15
46	1	TP2	SIP2	TP2
47	1	2.2uf	SM1206_T	C40
48	1	LT1026IS8	SMD8A_M	U8
49	1	REF198	SMD8A_M	U2

Total number of components: 102

LM34:

Item	Count	Label-Value	Pattern	Designation(s)
1	4	1N4148	SM1206_T	D2,D2,D3,D4
2	2	18K	SM1206_T	R1,R2
3	1	LM34-BOX	SIP3	LM34-BOX
4	2	Jumper	SM1206_T	J,J
5	1	1.0uf	SM1206_T	C3
6	2	0.1uf	SM1206_T	C1,C2
7	1	LM34-CPU	SIP3	LM34-CPU
8	1	REF191	SMD8A	U2
9	1	MCP3302	SMD14A	U1
10	1	SPIA	SIP6	SPIA

Total number of components: 16

GPS:

Item	Count	Label-Value	Pattern	Designation(s)
1	1	TRIMBLE GPS	TRIMBLE GOOD	GPS1
2	1	0.1uf	SM1206_T	C1
3	1	GPS	SIP5	GPS

Total number of components: 3

Apparatus Testing

Prior to receipt of the flight scintillation assemblies from Saint-Gobain, a smaller detector was built with components purchased through E-Bay. This unit was used to test the payload electronics without endangering the flight assemblies. During this testing phase it was found that there was a possibility of electrical arcing from the high voltage circuit in low temperatures and pressures such as would be seen during the balloon flight. This possibility was eliminated using a high dielectric strength epoxy (MG Chemicals 832HT, 1138 Volts / mil) over areas on the circuit board where high voltage arcing could occur. The voltage divider sockets of the PMTs, which were used in flight, were potted in epoxy leaving no exposed wiring. The completed package was

placed in a vacuum chamber and exposed to pressures low enough to expose any arcing. None were found.

Prior to flight operations, the payload was tested using Co^{60} and Na^{22} 1.0 μCi radiation sources purchased from Canberra Industries of Oak Ridge, TN. The radiation level of these sources was below the threshold specified by US Nuclear Regulatory Commission for which a Radiation Safety Officer is required. The radiation tests were performed to ensure proper operation of the photomultipliers and coincidence circuits. Co-60 and Na-22 were selected for testing because of they release high energy gamma rays approximately equal to the energy of inbound cosmic rays (Co^{60}:1173.2 keV, 1332.5 keV; Na^{22}: 511.0 keV, 1274.5 keV). During this testing it was found that one of the photomultipliers was not properly attached to its scintillator paddle. This problem was quickly repaired using Saint-Gobain Crystals BC-600 optical cement.

System Errors

Integration

After testing was successfully completed, the payload was integrated to the HASP platform at the Columbia Scientific Balloon Facility in Palestine, TX on July 24, 2007. During this time, two significant payload problems were uncovered and corrected. These problems were all related to the interface with the HASP platform.

The most severe problem discovered at the time of integration was an excessive transient current at startup. The payload was limited to 0.5 amps maximum current by the HASP. While confirming proper payload communication with the HASP platform that the payload startup current instantaneously peaked at 0.75 amps before receding to proper operating current of 0.285 amps. This transient was due to the startup of the 12 Volt power supply. The problem was corrected by adding a 10Ω current limiting resistor between the HASP and the payload. This problem could also have been resolved by replacing the fast blow fuses on the HASP with slow blow fuses; however, this was not an option.

A second problem discovered during integration was the communications between the payload and the HASP platform was not the correct levels. This was determined to be the result of an error in the documentation provided by HASP management. It was assumed that the payload-platform interface was to be at standard TTL levels, however, it was to be at standard RS-232 levels. This problem was corrected by the inclusion of a TTL to RS-232 level converter that was used during the testing phase to communicate with a bench top PC.

Flight

During the flight of the HASP, the payload experienced several failures. These failures were unexpected and cannot be thoroughly explained. The most severe of these failures was the payload ceasing to operate properly by entering a test mode that should not have been entered. The cause of this failure is unknown and could not be reproduced on the ground. It is believed that a high-energy ion strike was the likely cause of this fault. This error occurred twice during the duration of the flight. A successful recovery was completed from the first occurrence by cutting power to the payload and restoring it a minute later. This method did not work for the second occurrence of this error.

A less severe failure was the payload unexpectedly repeating its startup cycle throughout the flight. It is believed this was due to power lapses from the HASP platform supply; however, data was not sampled fast enough to catch these lapses. A final failure experienced during the flight was the replacement of the lead character in all data strings with a random character. As with the entry into the testing mode, the cause of this failure is unknown, but likely due to a high-energy ion or neutron strike in the upper atmosphere. The likelihood of these failures being the result of an ion strike is highly probable as has been found in other studies, such as a 1998 study of neutron strike effects on avionics conducted by Boeing (5). Even with these failures, the payload collected good data for 11.3 hours. This data included the ascent and 9.2 hours at float. Figure 8 shows an image from the CosmoCam of the completed payload during the flight.

Figure 8: Completed Payload at Float

Post Flight

After the flight the payload was inspected for signs of malfunction. Several items were noted; however, none should have caused a serious problem. The package showed signs of harsh mechanical treatment during landing and recovery, as can be seen in figure 9. The outside of the box was covered with mud, the box bottom plate was disconnected for the main outer shell, and the 10Ω current limiting Dale resistor, which was mounted externally, was found inside the package.

Figure 9: Payload after Recovery

During the flight the first character in the identification string sent from the package changed from a "W" to a "_". The text message used was stored in the PIC processors EEPROM. This most likely changed when the processor was updating the point count in EEPROM during a loss of power. Attempts to communicate with the board using the MAX-232 installed inside the package failed. The internal unit was replaced by the pre-flight external unit and communications between the package and PC were established.

The connections between the board and photomultiplier tubes had been strained and the dielectric epoxy showed signs of chipping. No exposed metal could be seen and no signs of arcing were present. All the solder connections (except those under the high dielectric epoxy) were inspected with a magnifying glass for signs of bad connection. None were found. There was some oxidation on the copper traces and solder mounds around through holed and surface mount connections; this was likely the result of the HASP landing in a freshly irrigated field in Southern California.

Upon return to West Virginia, the package was instrumented with a 500 mA FS current meter (Simpson 260 VOM) in series with the 28 Volt positive lead up stream from the 10Ω resistor and a Fluke model 12B multimeter was connected across the 10Ω

to measure the voltage drop. The serial data cable of the board was connected to a PC running the HASP host mode software. Using this set up the following was observed:

The current in the resistor as indicated by the voltage drop across the resistor and the current measured by the current meter was in line with Ohm's law for a 10Ω resistor for all measurement conditions. The resistor was cooled and heated. The leads to the resistor were pulled and twisted. None of these conditions caused the resistor to behave as anything except an Ohmic device. It appears the resistor was not a problem.

The measured currents to the board showed fluctuations inconsistent with the values measured before the flight. The nominal operating current was about 140-150 mA. The after flight current had a three modal character, where most of the time the current was at a nominal value of 140 mA. A second mode had the current at 350-400 mA, which is much too high and caused the 10Ω resistor to heat. A third mode had a current of about 50 mA and was the least frequently observed. The board was cycled off/on, twisted, bent, probed, and poked in an attempt to establish a pattern to mode change; however, none was found. These current modes were not observed during preflight testing.

The control voltage to the high voltage power supply was set to 3.265V prior to the flight. This supplied the photomultiplier tubes with about 977V (control input maps 0-5V to 0 to 1500V). The control voltage measured in the post flight inspection was 3.260V giving a calculated high voltage of 978V. These values appear to be in order.

Operation of the photomultiplier tube scintillation detectors, however, appeared to be bimodal (working and non working). The high dielectric epoxy was removed from the high voltage terminal of the power supply. The voltage on the exposed terminal was measured giving the following results:

The high voltage measured was 503V with the photomultiplier tubes connected. This value is inconsistent with the control voltage and the before flight measurements.

This is a true malfunction! The outputs from the photomultiplier units were removed one at a time to determine if there was a change in the high voltage. None was noted.

The PCB trace from the high voltage connection on the power supply to the board connections to the photomultiplier was cut to isolate the load from the power supply. The measured high voltage when isolated from the load was 972V which is consistent with the measured control voltage and the pre-flight high voltage measurement. It would appear there was some problem with the one or both of the photomultiplier units.

The high voltage was reconnected to the photomultiplier tubes. To further isolate the problem the high voltage bypass capacitors for each of the photomultiplier tubes were disconnected. The high voltage did not return to the correct value. Next the high voltage traces to each of the photomultiplier tubes were cut. This established that only one of the tubes caused the high voltage to be low. The 28V current with only the "good" tube working was 60 mA.

Results

The flight of the WVU detector, while it did not yield a complete set of data, provided enough data to generate the plot shown in figure 10. This plot, which shows that the rate of coincidence data versus atmospheric depth, bears a close resemblance to the Pfotzer curve, which is shown in figure 11. The peak of both the WVU curve and the Pfotzer curve occurs at approximately 55,000 ft. It was shown by Haymes and Korff in 1960 that the peak incidence of slow neutrons occurs around 60,000 ft (7), and by McDonald and Webber that the peak incidence of protons occurs around 50,000 ft (8). Since the main component of cosmic ray showers are hydrogen atoms that have been stripped of their electrons, it is valid to assume that the WVU and Pfotzer peaks are a combination of these peaks. It should be noted that the count rate on the WVU curve was measured in coincidences per 10 seconds; whereas, the count rate of the Pfotzer curve was measured in coincidences per minute.

Another significant difference between the Pfotzer and WVU curves is the normalized peak coincidence rate. The peak for the WVU curve occurs around 1800 coincidences per minute whereas the Pfotzer curve peaks at around 70 coincidences per minute. This difference is due to the size and efficiency of each detector. The Pfotzer curve was generated by data taken using Geiger-Mueller tubes, which have a smaller aperture of measurement than the scintillation detector used by WVU. While it would seem from the figures 10 and 11 that they were dimensionless, they are really a function of the surface area of the detector.

Figure 10 also shows the model developed by Dr. G. Michael Palmer, Emeritus Professor at West Virginia University, which was explained earlier. It can be seen in this plot and in figure 12 that the model is a very close fit to the experimental data.

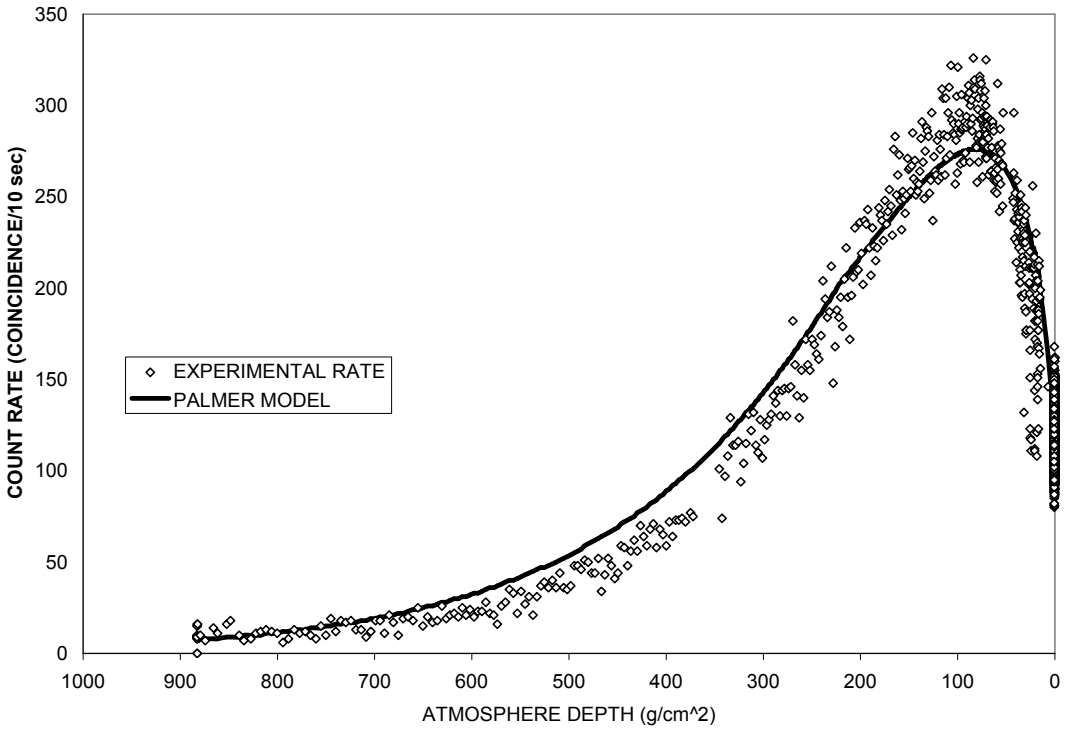

Figure 10: Experimental Coincidence Rate and Palmer Rate Model versus Atmospheric Depth

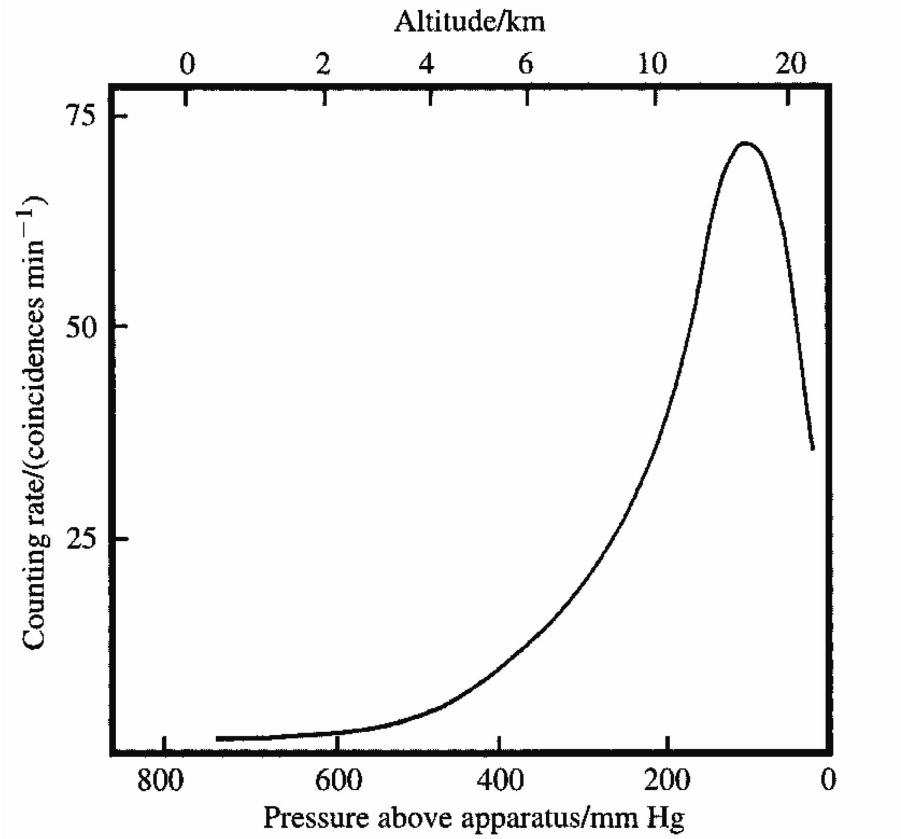

Figure 11: Pfotzer Curve (9)

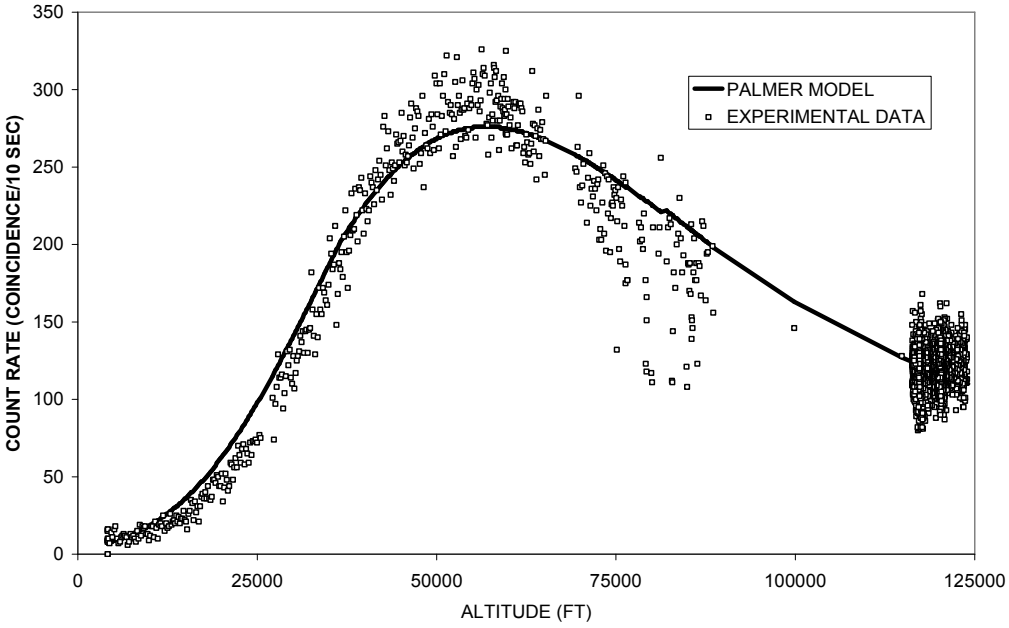

Figure 12: Coincidence Rate and Palmer Model versus Altitude

The isotropic count rate for the WVU detector was found to be 1752.45 ± 5.47% strikes per 10 second period. This was found by calculating the solid angle of detection, which was approximately equal to 2.158sr, and by using a maximum coincidence rate of 300 counts per 10 second period from figure 10. This rate was confirmed by the isolated count rates from both Channel A (figure 13) and Channel B (figure 14), which both peak within the predicted error margin. The predicted error is due to the inclusion of machining errors in the materials used to construct the detector, thus affecting the solid angle. The low coincidence/count rates above 75000 feet in figures 11, 13, and 14 are all the result of processor dropouts due to HASP power resets during that respective count period. The bunched data at 125000 feet on figures 11, 13, and 14 represent the 9.2 hours of data obtained by the payload at float altitude.

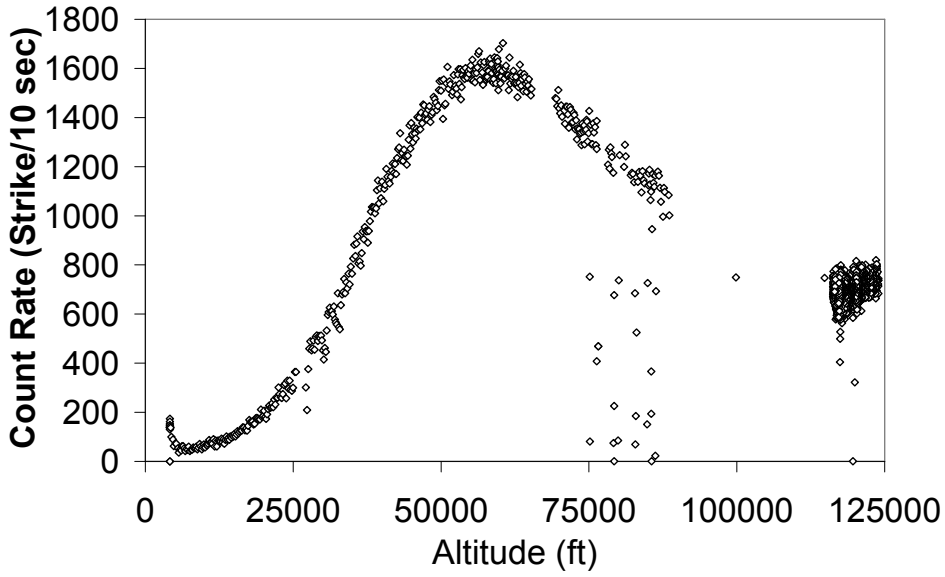

Figure 13: Channel A Incidence Rate versus Altitude

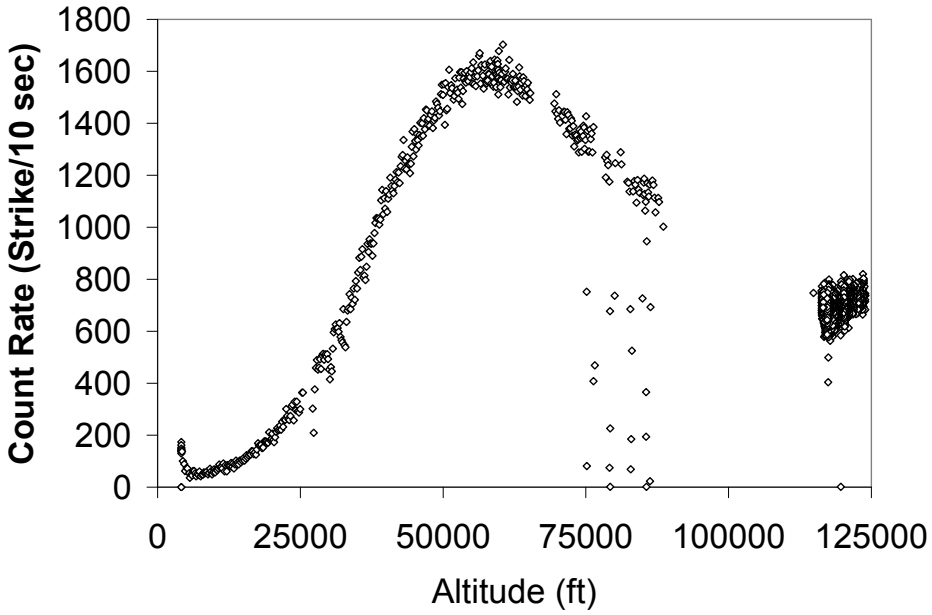

Figure 14: Channel B Incidence Rate versus Altitude

Conclusions

The flight of the WVU detector could be considered a successful failure. While the payload had several faults during the flight, the data during ascent was complete to around 80,000ft, which allowed for a confirmation of the Pfotzer curve to be made. The data recovered during the float period, when paired with the data obtained prior to the ascent failure, allowed for the confirmation of the model developed by Dr. G.M. Palmer. Had the data for the descent also been available, it should have been a mirror image of the ascent data, except for the coincidence percentage that was of solar origin, since the flight terminated around 3am.

References

1. National Aeronautics and Space Administration. “The History of Cosmic Ray Studies, 1900-1949”. http://helios.gsfc.nasa.gov/hist_1900.html
2. Friedberg, W., Copeland, K. “What Aircrews Should Know About Their Occupational Exposure to Ionizing Radiation”. Civil Aerospace Medical Institute, Federal Aviation Administration. Oct. 2003
3. World Health Organization. “Cosmic Radiation and Air Travel”. Nov. 2005 http://www.who.int/ionizing_radiation/env/cosmic/WHO_Info_Sheet_Cosmic_Radiation.pdf
4. Department for Transportation for the United Kingdom. “Protection of Aircrew from Cosmic Radiation.” May 2003. http://www.dft.gov.uk/pgr/aviation/hci/protectionofaircrewfromcosmi2961
5. Normand, E. “Single Event Effects in Avionics”. Boeing Defense and Space Group. 1998.
6. Nave, C.R. Hyperphysics. Georgia State University 2006 http://hyperphysics.phy-astr.gsu.edu/hbase/astro/imgast/cosparticle.gif
7. Haymes, R.C. and Korff, S.A. “Slow Neutron Intensity at High Balloon Altitudes”. Physical Review Vol. 120 No. 4 pp. 1460-1462 (Nov. 1960)
8. McDonald, F.B. and Webber W. R. "Proton Component of the Primary Cosmic Radiation", Phys. Rev. 115, 194, (1959)
9. Pfotzer, G. *Z. Phys.* 102**,** 23 (1936).

Appendix

HASP Post Flight Suggestions for Change

Add "soft start" circuit to the package to keep the 28V current below the 500 mA limit. This could be in the form a simple series resistor or an active circuit depending on the normal steady state current.

Add a reset supervisor that monitor the 12V supply and provides a "hard" reset when the voltage drops below a preset value and holds the PIC in reset until the voltage rises above a second (higher) preset value. The built in hysterisis will insure clean reset operation.

Provide a voltage divider to deliver a sample of the high voltage to monitor and archive in the data record. This will indicate any malfunction in the high voltage during operations.

The 2007 package stored the cumulative counts for each of counting categories. This did present some problems in data analysis when there were missing records or in flight resets. Storing only the counts in the current data period would be more efficient and simplify the data analysis.

Place the program mode switch on the exterior pf the package where it could be accessed at any time. This would allow the package to enter test mode without opening the box. One would have to insure that the mode switch were in the correct position before launch.

There was simple miscommunication about the serial port levels that led to the non-inclusion of the RS-232 converter. In the next version this would be onboard.

Provide for program mode verification in the operational program loop. During the flight the program malfunction getting out of the operational loop and entering the

test loop. This error could be corrected by looking at the mode switch (jumper) in both the operational and test loops every time through. This would only cost about 2 μs per loop through. If the program finds it is in the test loop when the mode switch indicated it should be in the operational loop force a "cold" reset.

There were no command inputs from the HASP processor used in the 2007 package. In hindsight this was a mistake. The next version of the WVU HASP package will include HASP commands to allow reset and other house keeping functions.

It may also be prudent in future missions to shield the payload electronics from high-energy ion strikes. This, however, is only a feasible option if the payload weight limit were increased above 1 kg.